*Sensors and Materials*, Vol. 35, No. 9 (2023) 3125–3135
MYU Tokyo



S & M 3379

# Geometric Modeling and Estimation of Robotic Fin Shape with Bending Actuators and Passive Elements

Noriyasu Iwamoto*

Faculty of Textile Science and Technology, Shinshu University, Tokida 3-15-1, Ueda, Nagano, 386-8567, Japan

(Received March 15, 2023; accepted May 18 2023)

***Keywords:*** bio-inspired robots, fin model, shape estimation, constant mean curvature surfaces

One possible design approach for bio-inspired robots is to employ structures that facilitate their shape estimation to enable control that mimics the animal's locomotion. We propose a discrete surface model for surface-shaped body parts of bio-inspired robots and a method for computing its shape. The surface model is constructed by alternately connecting bending actuators and passive elements. This study focused on a robotic stingray, and its fins were fabricated from cylindrical bending actuators with living hinges and fabric. The proposed computation takes about 10 ms, short enough to allow real-time computation. The shapes were estimated from the actuator's control value obtained in experiments, and the results were compared with the measurement results using an optical motion capture system. The differences between the estimated and measured point positions were within 15 mm, suggesting that a more accurate estimation is possible with robot system improvements. If actuators for a bio-inspired robot are surface-shaped, as in soft or bio-hybrid actuators, this fin model is expected to be a helpful reference for robotic design.

## 1. Introduction

Surface-shaped body parts of animals interact with the fluid surrounding them, and inseparable relationships exist between their shape and the efficiency of the animal's locomotion:[1,2] for example, the wings of insects, birds, and bats, the fish fins, and the jellyfish body. In robotics, fully imitating a biological body is not necessarily a preferred approach. Robot configurations involve a trade-off between the size and capabilities of existing computers, actuators, sensors, and implementation methodologies. Theoretically, the controllability and observability of the robotic system are prioritized. In these cases, an approximate approach to the biological body is employed. For many studies, surface parts are typically assembled from rigid or elastic materials that are directly actuated and flexible elements that passively follow them. This assembly can be regarded as a problem in discretizing a surface, and the arrangement of the rigid and elastic materials often follows the original animal's skeleton.

Herein, we focus on the pectoral fins of stingrays, which are highly expressive in shape, and on the robotic fin inspired by them. The pectoral fins of rajiformes generate undulating motion

*Corresponding author: e-mail: iwamoto@shinshu-u.ac.jp
https://doi.org/10.18494/SAM4387

ISSN 0914-4935 
https://myukk.org/

along the body and bending deformation in the spanwise direction.[3] The two fins on the left and right are moved symmetrically to achieve forward motion and asymmetrically to produce turning motion.[4] Some robotic stingray designs focus only on the undulating motion, with rigid rods placed at equal intervals along the body and controlled up and down in phase-shifted motions.[5–7] These robotic fins are fabricated by filling the space between the rods with passive flexible elements such as silicone rubber. To produce the spanwise deformation, silicone rubber, wide enough to cover the rods completely, is curved by fluid resistance, or an elastic material is employed for the rods.[8,9] In the minimal system configuration design, only one rod moves the passive flexible fin, utilizing the wave propagation of the fins.[10,11] A robot that more closely mimics the stingray's body structure has been developed by combining muscles made of rat cardiomyocytes and an elastic frame.[12] In this robot, the elastic frame stores elastic energy as the muscle bends, and the energy is utilized for bending in the opposite direction.

To simulate the locomotion of an animal, not only a robotic structure but also a model capable of representing the surface shape and a method for estimating it are helpful because the shape influences the fluid flow. Passive membrane parts driven by rigid rods can be easily modeled as linearly complementary surfaces between the rigid rods.[7] When a robot has a soft or biohybrid actuator, the actuator domain shape is a surface,[12,13] and several models are conceivable. Collectively representing actuators and passive elements requires finding a function to describe all possible shapes of the surface. Interpolating functions with control points, such as B-spline surfaces, involves three times as many variables as the number of control points to vary in accordance with the actuator's shape, which is counter-intuitive. When dividing a surface region into several patches, adjacent patches must satisfy the condition that their boundary positions coincide. If an actuator is modeled as a patch, we are faced with the problem of how to satisfy the condition in a structure with a series of actuators.

In this paper, we will propose a simple and expressive discrete surface model for the fins of a robotic stingray composed of bending actuators and passive elements alternately bonded (Fig. 1). This model can be characterized as an extension of the linearly interpolating surface model between rigid rods. If the shapes of all bending actuators can be estimated from the sensor system, the shape of the passive elements can be obtained, resulting in the recovery of the entire fin shape. Additionally, we will show that the computational time of around 10 ms required for shape estimation is short enough to enable real-time computing. Finally, we will discuss that this fin model has an attractive mathematical property.

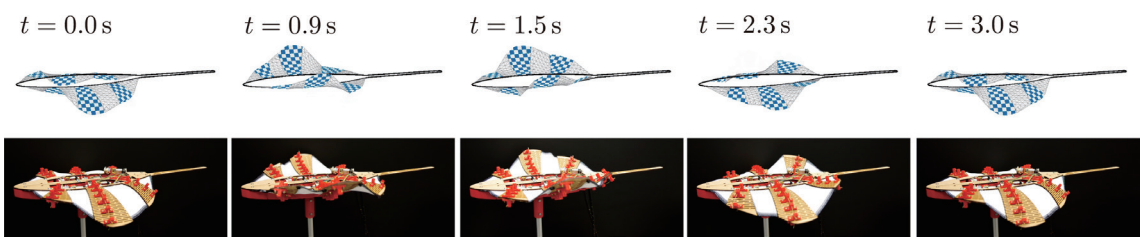


Fig. 1. (Color online) Snapshots of fins of the robotic stingray driven by sin waves and the estimated fin shape.

## 2. Materials and Methods

### 2.1 Design of robotic stingray

Figure 2(a) shows the developed robotic stingray, which is 468 mm long, 300 mm wide, and 48 mm thick [Fig. 2(b)]. The fins of the robot have actuators that bend in a cylindrical shape and fabric that deforms passively, arranged alternately along the body. The actuators and passive elements on the right side are named RA1 to RA3 and RP1 to RP4, respectively, as shown in Fig. 2(b).

#### 2.1.1 Cylindrical bending actuator

A cylindrical bending actuator is realized using a medium-density fiberboard (MDF) with living hinges,[14] a motor, Kevlar thread, and poles with a hole for the thread. Six cylindrical bending actuators were designed symmetrically to the robot's body, and straight-line living hinges were formed on a 2.5-mm-thick MDF using a laser cutter. The hinge's holes are 18 mm long and 0.6 mm wide and are spaced 20.8 mm apart in the nonbending direction and every 3 mm in the bending direction.

A typical tendon-driven system is used to drive the cylindrical bending actuator. A DC-geared motor with a gear ratio of 298:1 (Pololu, stall torque of 3.4 kg·cm at 6 V drive) is connected to a pulley with a diameter of 9.25 mm, which winds the Kevlar thread. The Kevlar thread reaches the pulley from the tip of the MDF through some holes of the poles [red-colored parts in Fig. 2(a)], and the pole's hole is set at 10 mm from the MDF. The poles are placed along the bending direction of the MDF on both the top and bottom of the MDF. In this system, as the

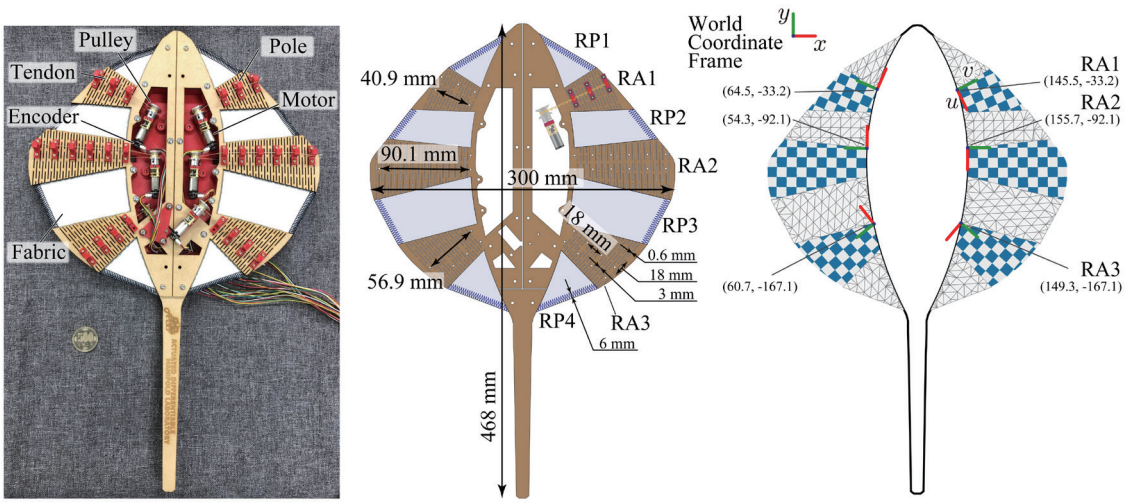


(a) (b) (c)

Fig. 2. (Color online) (a) Flexible robotic fin with cylindrical bending actuator and fabrics, (b) its main dimensions, and (c) position and orientation of coordinate systems for shape estimation.

motor rotates forward, the Kevlar thread along the top is pulled, and that along the bottom is relaxed. When the motor rotates in the opposite direction, the relationship between the two is reversed. Therefore, the actuator can bend in both the top and bottom directions.

The DC-geared motor is equipped with a rotary magnetic encoder. By integrating the encoder value, the rotational angle of the pulley and the change in the Kevlar thread length can be determined; from these, the curvature of the MDF can be estimated. Figure 3(a) shows the relationship between the rotational angle of the pulley and the MDF shape in the actuator RA2. Fitting a circle to each deformation result in Fig. 3(b) shows that this actuator can be sufficiently approximated as a cylinder. In this case, the rotational angle of the pulley and the curvature of the MDF appear to have a linear relationship whose slope depends on the MDF length [Fig. 3(c)]. Geometrically, ignoring the pole's width, let $\theta$ be the rotational angle of the pulley and $\kappa$ be the curvature of the actuator. Then the relationship between $\theta$ and $\kappa$ can be expressed as

$$\theta = \frac{1}{R}\left( s - 2n\left( \frac{1}{\kappa} - \alpha \right) \sin \frac{\kappa s}{2n} \right), \tag{1}$$

where $R$ is the pulley radius, $\alpha$ is the height of the pole's hole, and $n$ is the number of spaces between the poles. The variable $s$ denotes the MDF length, and $s$ for each fin is shown in Fig. 2(b). The dotted lines in Fig. 3(c) represent the curvature $\kappa$ obtained from Eq. (1). Unlike the geometrical equation, a dead band occurs near the pulley angle of 0 degrees due to the slack in the tendon. Moreover, the friction between the pole's holes and the thread causes the change in thread length to be less evenly distributed among the poles, which tends to reduce the slope.

Three DC-geared motors are connected to a microcontroller (Arduino Mega 2560) via motor drivers (Toshiba, TB6612) and controlled by feedforward-feedback controllers with a control period of 20 ms. Let $\gamma$ be the gear ratio of a geared motor and $N$ the ratio of the voltage to the angular velocity of the motor. The voltage feedforward $V_f$ is defined by the proportional relationship of the control voltage and the angular velocity $\dot{\theta}$ as

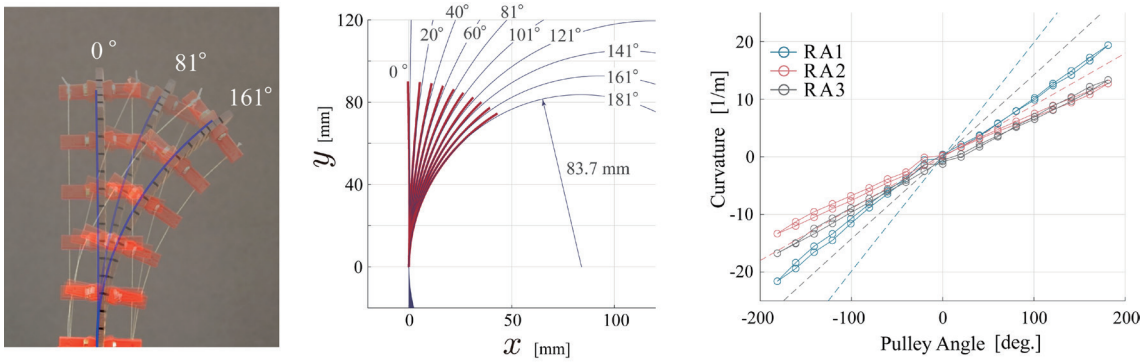


(a) (b) (c)

Fig. 3. (Color online) (a) Relationship between bending of the cylindrical actuator RA2 and the pulley angle, (b) result of fitting a circle to the MDF, and (c) relationship between the pulley angle and the curvatures of the cylindrical actuators.

$$V_f(\kappa, \dot{\kappa}) = \gamma N \dot{\theta}. \tag{2}$$

The angular velocity $\dot{\theta}$ is obtained by substituting the values of $\kappa$ and $\dot{\kappa}$ into the time derivative of Eq. (1). Given the target pulley angle $\theta_t$, the feedback control law is constructed so that the error between $\theta$ and $\theta_t$ is zero. Finally, the control voltage of the motor is given by

$$V = V_f + K_p(\theta_t - \theta), \tag{3}$$

where $K_p$ is the proportional gain and we set $K_p = 24.8$.

### 2.1.2 Passive element

For the passive element, a two-way tricot fabric made of 89% polyester and 11% polyurethane was used as a highly stretchable fabric. The fabric's physical properties were measured using a tensile and shear tester (Kato Tech, KES-FB1-AUTO-A). Figure 4 shows the measurement results. In tension, the fabric elongated 63.3% in the warp direction and 78.4% in the weft direction at 100 gf/cm. In shear, for both warp and weft directions, a tension of about 5.6 gf/cm is required to obtain a shear angle of 8°. This fabric supports the maximum elongation required by the deformations of the adjacent actuators and can be stretched by the force generated from the actuators.

The required size was cut from a piece of fabric, and a 6-mm-wide overcast stitch was applied to the edge of the fin's boundary using a double-needle lockstitch machine. Subsequently, the fabric's edges and the adjacent actuators' corresponding edges were glued together.

## 2.2 Modeling and estimation

Herein, the robotic fin is modeled with the bending actuator as a cylinder and the passive element as a surface with a minimum area spanning a given frame.

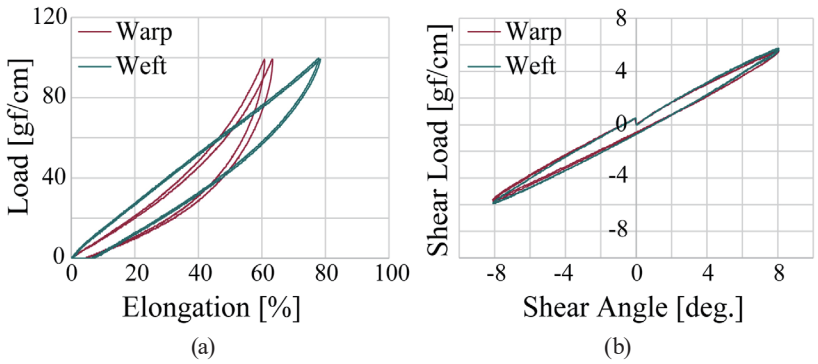


Fig. 4. (Color online) Physical properties for tensile and shear of two-way tricot fabrics employed as passive elements.

A world coordinate system is designated as shown in Fig. 2(c), and local coordinate systems are placed at each actuator and passive element. Let ($u$, $v$) be the local coordinates, and assume that the actuator bends in the $v$-direction. Then, the homogeneous transformation matrix $\boldsymbol{T}_{cy}$ between the local coordinate system of an actuator and the coordinate system at a point on the actuator can be written as

$$\boldsymbol{T}_{cy}(u,v)=\begin{bmatrix} 1 & 0 & 0 & u \\ 0 & \cos(\kappa v) & -\sin(\kappa v) & \sin(\kappa v)/\kappa \\ 0 & \sin(\kappa v) & \cos(\kappa v) & (1-\cos(\kappa v))/\kappa \\ 0 & 0 & 0 & 1 \end{bmatrix}. \tag{4}$$

When the curvature $\kappa$ is equal to zero, Eq. (4) cannot be expressed, so we replace the curvature $\kappa$ with an extremely small value.

The above model implies that the actuator's shape can be obtained if the curvature $\kappa$ can be estimated. As mentioned earlier, if the initial pulley angle is known, the pulley angle can be determined by integrating the encoder measurements. Moreover, the curvature $\kappa$ can be estimated from the pulley angle by using the equation, assuming the experimental results in Fig. 3(c) to be linear.

The passive elements are modeled as a shape function satisfying the Laplace equation with boundary conditions. Let $\boldsymbol{f}: \mathbb{R}^2 \rightarrow \mathbb{R}^3$ be the shape of a passive element, and for a given boundary shape, we find $\boldsymbol{f}$ such that the area inside the boundary is minimized. For example, in RP2, one of its four edges borders the body, and two adjoin each actuator. Since the shape of the remaining edge, which is the fin boundary, has not been determined, for simplicity, we assume that this edge is a straight line connecting the corners of two adjacent actuators. The surface with the minimum area is that on which the following stretch energy of a membrane fixed to the boundary shape is the lowest.

$$E_s = \iint_U \left\| \frac{\partial \boldsymbol{f}}{\partial u} \right\|^2 + \left\| \frac{\partial \boldsymbol{f}}{\partial v} \right\|^2 du dv \tag{5}$$

Here, $U$ denotes the domain of the passive element. The Euler–Lagrange equation of Eq. (5) is

$$\Delta_S \boldsymbol{f} = \boldsymbol{0}, \tag{6}$$

where $\Delta_S$ is the Laplace–Beltrami operator. Equation (6) with a boundary condition can be expressed as a simultaneous equation using the cotan-Laplacian for a triangular mesh,[15] and $\boldsymbol{f}$ can be obtained by solving the simultaneous equation.

If the shapes of all bending actuators can be determined, the boundary shapes of each passive element part are automatically determined, and the shapes inside the boundaries can be estimated by solving Eq. (6) as many times as the number of passive elements.

## 3. Results and Discussion

### 3.1 Computational time for shape estimation

Since all actuator shapes demand practically little computational time from Eq. (4), the computational time of the proposed fin model depends on how precisely the passive elements are obtained. The estimation method in the previous section was implemented in MATLAB R2022a and run on a computer with an Intel Core i7-8565U CPU and 16 GB memory. This measurement of computational time does not include the control system of an actual robot. We randomly generated 100 pairs of curvatures for six actuators and estimated the fin shape with each pair. The maximum absolute curvature value was chosen to be one and the minimum to be $10^{-6}$. Figure 5 shows the average time taken to estimate eight passive elements, divided by 2, 5, 8, and 10 mm for the passive element region. The numbers of vertices and faces in the generated meshes are shown in Table 1. We can see that the estimated time for one passive element is on the order of $10^{-3}$ s from Fig. 5. The computational time for one actuator shape is even shorter, on the order of $10^{-4}$ s. The 10, 8, and 5 mm mesh sizes result in less than 10 ms calculations. For 2 mm, the computational time increases significantly with the number of mesh vertices. Although reducing the mesh size increases the resolution of the resulting surface, the rough shape remains the same, and the benefit of increased computational time is low.

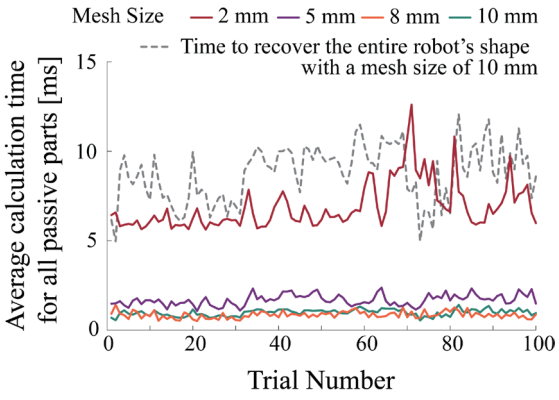


Fig. 5. (Color online) Average time needed for estimation of shapes of all passive elements.

Table 1
Number of faces and vertices of the triangular meshes of passive elements relative to mesh size.

| | 10 mm | | | | 8 mm | | | |
|---|---|---|---|---|---|---|---|---|
| | RP1 | RP2 | RP3 | RP4 | RP1 | RP2 | RP3 | RP4 |
| Number of faces | 41 | 77 | 121 | 61 | 53 | 103 | 171 | 81 |
| Number of vertices | 35 | 58 | 81 | 50 | 41 | 71 | 106 | 60 |
| | 5 mm | | | | 2 mm | | | |
| | RP1 | RP2 | RP3 | RP4 | RP1 | RP2 | RP3 | RP4 |
| Number of faces | 103 | 221 | 375 | 153 | 557 | 1239 | 2145 | 789 |
| Number of vertices | 66 | 130 | 208 | 96 | 293 | 639 | 1093 | 414 |

The dotted line shows the total estimated time for six actuators and eight passive elements with a mesh size of 10 mm. All trials are completed within 15 ms, allowing for a control cycle of 20 ms. Although the computation time varies depending on the mesh size representing a surface, it generally takes more than 1 s to integrate the moving frame on the surface [16] to reconstruct its shape. Considering this, we can see that the pair of the proposed fin model and estimation method allow for short computation times.

### 3.2 Comparison of model and robot shape

Figure 1 shows a series of robot deformation and the estimated shape at that time. We set a sin wave with a period of 3 s and an amplitude of 20 $m^{-1}$ as the target trajectory of the bending actuator. The phases were synchronized at the left and right fins and shifted by $\pi/3$ at RA1 and RA2 and at RA2 and RA3, respectively. The proposed fin, as a stingray, can simultaneously represent traveling waves along the body and radial bending. Practically, adjacent bending actuators cannot be directly connected because they have different curvatures during deformation, i.e., different boundary shapes of the actuators. In the proposed fin, a passive element is located between them, absorbing the difference in boundary shape. Furthermore, the estimated shape is qualitatively consistent with the deformed shape.

The usability of the estimation method can be demonstrated numerically from the measurement results by optical motion capture. We acquired the fin shape by measuring the positions of markers placed on the robot using a motion capture system (VENUS3D) and assumed the measured positions to be true values. The markers were placed for passive elements RP2 and RP3, as shown in Fig. 6(a). The sampling frequency of the motion capture system is 120 Hz. The positions of the measured markers were compared with those corresponding to the markers obtained by the estimation method from the encoder measurements. Figure 6 shows the measured marker position (red) and the shape and position estimated from the encoder values (blue). Panels (a), (b), and (c) show the results for the undeformed state, at time 12.5 s, and at time 16.7 s. Furthermore, Figs. 7(a) and 7(b) show the error between the measured and estimated positions for RP2 and RP3, respectively. The graphs from (i) to (iii) are shown for each column where the markers are located, numbered in order of proximity to the outside of the fin. The top row graphs in Fig. 7 show the curvatures of adjacent actuators; the solid line is the value

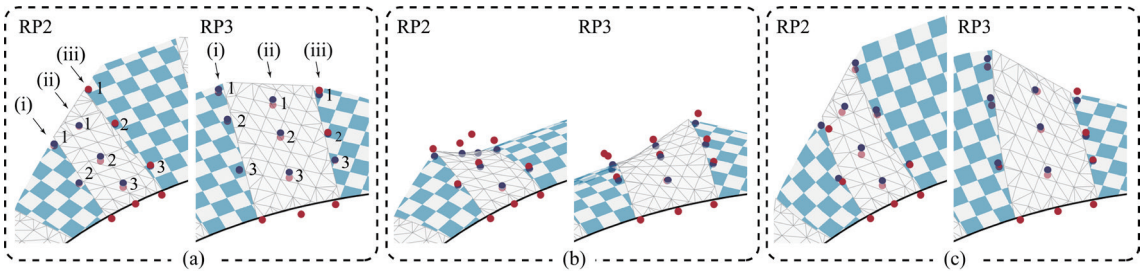


Fig. 6. (Color online) Marker positions on the fin measured by the optical motion capture system (red) and marker positions estimated from the encoder values (blue).

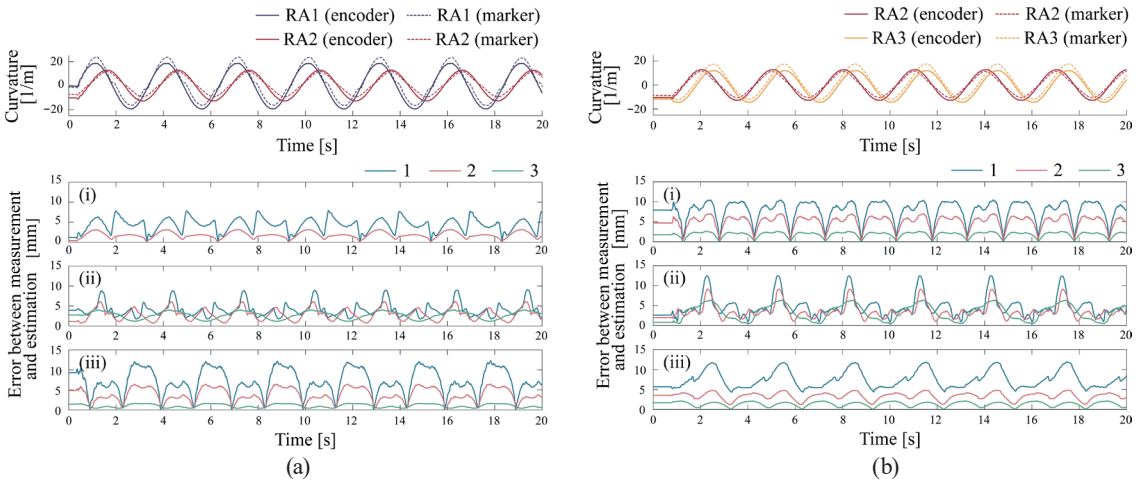


Fig. 7. (Color online) Estimated curvature of the bending actuator and the curvature obtained by fitting a circle from the markers (top graph), and errors between the measured and estimated positions of the markers [(i) to (iii)].

estimated from the encoder, and the dotted line is the value obtained by fitting a circle to the measured markers. We can see that all marker positions can be estimated with errors of less than 15 mm. In both (a) and (b), the errors in (i) and (iii) are due to estimation errors in the actuator's curvature, i.e., the difference between the solid and dotted lines in the top graph. The error is more significant for markers located outside the fin, and the time of maximum error coincides with that of the largest bending. Additionally, at points on the passive element (ii), we can see that the error is more significant when the curvatures of the adjacent actuators cross. When the two actuators' bending directions differed, slack in the passive element resulted in a deviation from the estimated position.

A more accurate shape estimation can be achieved through several improvements to the robot system. Since the accuracy of curvature estimation of a bending actuator is directly related to that of shape estimation, we need to introduce a sensor that can absolutely measure the curvature, such as a conductive stretch sensor. The slack in the passive elements can be eliminated by gluing the fabric in a pretensioned state. Another solution is expected to employ shrinking soft actuators to achieve a surface with the minimum area. We used a fabric as the passive element, but silicone rubber may also be used. However, if the silicon rubber is thick, deformation occurs in bending. Introducing combined energy with elongation and bending[15] in the shape calculation of passive elements would apply to the thick silicon rubber.

### 3.3 Piecewise constant mean curvature surface

The proposed fins can be considered a surface with piecewise constant mean curvature. A point on a surface and a tangent vector at that point define a curvature called normal curvature.[16] By fixing the point and changing the direction of the tangent vector, the maximum and minimum values of the normal curvature can be obtained. The maximum value $\kappa_1$ and

minimum value $\kappa_2$ are called principal curvatures, and the mean curvature $H$ can be defined from the average of the principal curvatures:[16]

$$H = (\kappa_1 + \kappa_2)/2. \tag{7}$$

For a cylinder of radius $r$, the principal curvatures are $1/r$ and 0, and the mean curvature is the constant value $1/(2r)$. The passive element was modeled as a locally minimum-area surface spanning a given boundary. This surface is called a minimal surface, and the mean curvature is zero everywhere on the surface. Therefore, this fin model assumes a piecewise constant mean curvature.

This assumption is similar to the assumption of piecewise constant curvature for continuum manipulators,[17] i.e., the idea of a curve connecting arcs. A wide variety of shapes can be represented by connecting sections of constant curvature, which provides a simple shape representation. Constant mean curvature surfaces include geometries such as planes, cylinders, spheres, catenoids, unduloids, and nodoids.[18] Furthermore, for geometries with nonzero mean curvature, the same kinematics theory as for rigid robots can be considered.[19] We expect to construct highly expressive fins using surface-shaped actuators capable of approximating these geometries. For surface-shaped body parts of bio-inspired robots, defined kinematics and shape estimation could achieve their advanced control and help mimic animal locomotion.

## 4. Conclusions

We proposed a surface model for bio-inspired robots. Using robotic stingray's fins, we confirmed the potential usefulness of the proposed model in shape estimation. The fins of the robotic stingray consist of alternately bonded cylindrical bending actuators and fabric. The fin shape can be estimated in two steps: (i) estimate all bending actuator shapes, and (ii) compute all fabric shapes from closed curves formed by actuator boundaries. The fin model allows the assumption of piecewise constant mean curvature to be applied. If the shape of a soft actuator or a biohybrid actuator can be fitted with a constant mean curvature surface, the proposed method can be applied to fins composed of such actuators and passive elements. The shape of this highly expressive fin may be controlled in real-time for digging sand on the seafloor. Therefore, our results will aid efficient exploration of mineral resources and marine life. In addition, the proposed model is expected to be extended to surface-shaped body parts of other bio-inspired robots.

## Acknowledgments

This work was supported by JSPS KAKENHI Grant Number JP21K14127.

## References


1 D. D. Chin and D. Lentink: J. Exp. Biol. **219** (2016) 920.
2 T. Y. Wu: Annu. Rev. Fluid Mech. **43** (2011) 25.
3 E. L. Blevins and G. V. Lauder: J. Exp. Biol. **215** (2012) 3231.
4 J. M. Parson, F. E. Fish, and A. J. Nicastro: J. Exp. Mar. Biol. Ecol. **402** (2011) 12.
5 R. Gliva, M. Mountoufaris, N. Spyridakis, and M. Sfakiotakis: Proc. New Horizons in Industry, Business and Education (2015) 81.
6 Y. Wang, J. Tan, and D. Zhao: J. Bionic Eng. **12** (2015) 204.
7 Q. Li, J. Zhang, J. Hong, D. Hu, Y. Yang, and S. Guo: J. Bionic Eng. **18** (2021) 812.
8 G. Shi and Q. Xiao: Eur. J. Mech. B/Fluids. **87** (2021) 75.
9 M. Yurugi, M. Shimanokami, T. Nagai, J. Shintake, and Y. Ikemoto: Sci. Rep. **11** (2021) 1.
10 P. V. Y. Alvarado, S. Chin, W. Larson, A. Mazumdar, and K. Youcef-Toumi: Proc. IEEE Int. Conf. Biomedical Robotics and Biomechatronics (2010) 473.
11 T. Li, G. Li, Y. Liang, T. Cheng, J. Dai, X. Yang, B. Liu, Z. Zeng, Z. Huang, Y. Luo, T. Xie, and W. Yang: Sci. Adv. **3** (2017) e1602045.
12 S. J. Park, M. Gazzola, K. S. Park, S. Park, V. Di Santo, E. L. Blevins, J. U. Lind, P. H. Campbell, S. Dauth, A. K. Capulli, F. S. Pasqualini, S. Ahn, A. Cho, H. Yuan, B. M. Maoz, R. Vijaykumar, J.-W. Choi, K. Deisseroth, G. V. Lauder, L. Mahadevan, and K. K. Parker: Science, **353** (2016) 158.
13 K. Takagi, M. Yamamura, Z. W. Luo, M. Onishi, S. Hirano, K. Asaka, and Y. Hayakawa: Proc. IEEE/RSJ Int. Conf. Robotics and Systems (2006) 1861.
14 T. Ohshima, T. Tachi, H. Tanaka, and Y. Yamaguchi: Proc. Int. Assoc. Shell Spat. Struct. Symp. (2015) 1.
15 M. Botsch and O. Sorkine: IEEE Trans. Vis. Comput. Graph. **14** (2008) 213.
16 M. P. do Carmo: Differential Geometry of Curves & Surface (Dover Publications, New York, 2016).
17 R. J. Webster III and B. A. Jones: Int. J. Rob. Res. **29** (2010) 1.
18 K. Kenmotsu: Surfaces with Constant Mean Curvature (Amer Mathematical Society, Washington, D.C., 2003).
19 N. Iwamoto: Proc. IEEE/SICE Int. Symp. System Integration (2023) 284.